
Article:
Al-Sunna, R., Pilakoutas, K., Hajirasouliha, I. et al. (1 more author) (2012) Deflection behaviour of FRP reinforced concrete beams and slabs: An experimental investigation. Composites Part B: Engineering, 43 (5). 2125 - 2134. ISSN 1359-8368

https://doi.org/10.1016/j.compositesb.2012.03.007

Al-Sunna R, Pilakoutas K, Hajirasouliha I & Guadagnini M (2012) Deflection behaviour of FRP reinforced concrete beams and slabs: An experimental investigation. *Composites Part B: Engineering*, 43(5), 2125-2134.

Deflection Behaviour of FRP Reinforced Concrete Beams and Slabs: An Experimental Investigation

Raed Al-Sunna[a], Kypros Pilakoutas[a], Iman Hajirasouliha[b*], Maurizio Guadagnini[a]

[a] *Department of Civil & Structural Engineering, The University of Sheffield, Sheffield, UK*

[b] *Department of Civil Engineering, The University of Nottingham, Nottingham, UK*

[*]Corresponding author, e-mail: i.hajirasouliha@nottingham.ac.uk

ABSTRACT

The flexural response of FRP RC elements is investigated through load-deflection tests on 24 RC beams and slabs with glass FRP (GFRP) and carbon FRP (CFRP) reinforcement covering a wide range of reinforcement ratios. Rebar and concrete strains around a crack inducer are used to establish moment-curvature relationships and evaluate the shear and flexural components of mid-span deflections. It is concluded that the contribution of shear and bond induced deformations can be of major significance in FRP RC elements having moderate to high reinforcement ratios. Existing equations to calculate short-term deflection of FRP RC elements are discussed and compared to experimental values.

Keywords: A. Carbon fibre; A. Glass fibre; C. Analytical modelling; D. Mechanical testing; Deformation behaviour.

1- Introduction

FRP reinforcement for concrete has been developed to replace steel in special applications, particularly in corrosion-prone RC structures. Under similar conditions, in terms of concrete strength, applied loading, member dimensions and area of reinforcement, FRP RC members are expected to develop larger deformations than steel reinforced members [1]. This can be mainly attributed to the lower modulus of elasticity of the FRP rebars, but also to their unique bond characteristics. As a result, the design of FRP RC elements is often governed by the serviceability limit state [2]. Accurate calculation of service deflections can be done through integration of curvatures [3, 4] and making allowance for shear and bond deformations. However, such calculations are time consuming and not suitable for design. It is therefore important to develop simplified design methods to evaluate the deflection of RC elements with an acceptable accuracy. The implementation of simple elastic analysis models, along with the use of an

effective moment of inertia to describe the reduced stiffness of a cracked element, has proven effective in determining service deflections of steel reinforced concrete elements and has also been adopted for FRP reinforced concrete elements. ACI 440.1R-06 [5], for example, has adopted a modified form of the effective moment of inertia equation included in ACI 318 [6] and originally developed by Branson [7]. Although a similar model is also discussed in the design manual published by ISIS Canada [8], the use of an equation derived by implementing the tension stiffening effect included in Model Code 90 [3] is proposed as a more reliable model for concrete elements reinforced with different types of FRP reinforcements. The tension stiffening model of Model Code 90 also underlies the method recommended in Eurocode 2 [9] to estimate service deflections for steel RC elements, and was shown to lead to acceptable results also for FRP RC elements [4]. CAN/CSA-S806 [10] recommends determining deflections by integration of curvatures along the span, but ignores the tension stiffening effect provided by the FRP reinforcement. Instead it proposes the use of a gross and cracked moment of inertia to represent the stiffness of un-cracked and cracked portions of the element, respectively.

Although the code approaches for the prediction of short-term deflection account for a reduced flexural stiffness of the element due to cracking [11], this effective stiffness is treated as a global parameter and cannot capture the effect of localised cracking. As a result, the deflection derived using only cracked moment of inertia is expected to provide an upper bound limit for short-term deflections. However, tests on beams and slabs [12, 13, 14] show that deflections tend to exceed this upper bound even at relatively low load levels, when shear deformation or de-bonding are not expected to be of significance.

Shrinkage can also contribute to deformations [14, 15] due to the restrain provided by the flexural bars in the bottom of the beams and the consequent development of a shrinkage-induced curvature. Since the stiffness of FRP bars is considerably lower than that of steel, this restrain is not as high as for an equivalent steel reinforced section. Nonetheless, any restraint can cause the development of micro cracks in the concrete and, as such, will have an impact on the apparent tensile strength of the concrete in the structural element. However, beyond the initial impact around the cracking load, shrinkage strains cannot justify deflections larger than predicted by the fully cracked section.

The plane sections remain plain assumption of section analysis is considered true for flexural elements at the macro scale, but it does not necessarily apply in the regions around the crack. This may be amplified in the case of FRP RC since the neutral-axes depth can be very small. However, results from

lightly steel reinforced concrete elements show that there are no significant additional deformations at least up to the point of yielding [16].

Mota et al [17] and Rafai and Nadjai [18] examined several existing deflection models for FRP RC beams and slabs and concluded that their performance is highly dependent on the accuracy of the calculated cracking moment. The results of their study indicate that there is a critical need for reliability analysis of FRP code equations to develop more accurate load-deflection formulas for FRP RC members.

Despite extensive research on the behaviour of FRP RC members, less research has been conducted on deflection prediction of FRP RC elements considering the effects of different stress levels and reinforcement ratio (for example [19] and [20]). To examine these, an experimental study was undertaken to investigate the deflection behaviour of FRP RC concrete beams and slabs at service ability and ultimate load levels. The experimental programme comprised twelve beams and twelve slabs with glass FRP (GFRP) and carbon FRP (CFRP) with a wide range of reinforcement ratios. The experimentally determined deflections are used to examine the accuracy of the predictive models discussed above and presented in detail in the following sections.

2- Deflection prediction of FRP RC elements

To calculate short-term deflections of FRP RC beams, ACI 440.1R-03 [21] adopts the following expression for effective moment of inertia (I_e), which accounts for the lower FRP modulus of elasticity (E_f) and different FRP bond characteristics.

$$I_e = I_{cr} + \left(\beta_d I_g - I_{cr}\right)\left[\frac{M_{cr}}{M_a}\right]^3 \le I_g \tag{1}$$

$$\beta_d = \alpha_b\left[\frac{E_f}{E_s} + 1\right] \tag{2}$$

where I_g and I_{cr} are the gross and cracked moment of inertia; M_{cr} and M_a are the cracking and applied moment; E_f and E_s are the FRP and steel modulus of elasticity respectively; and α_b is a bond dependent coefficient, which equals 0.5 for steel rebars. In the absence of more research data, a value of 0.5 has been recommended for all FRP rebar types. ACI 440.1R-06 [5] abandons the reliance of β_d on bond, and takes β_d as proportional to the ratio of reinforcement ratio (ρ_f) to the balanced reinforcement ratio (ρ_{fb}).

$$\beta_d = \frac{1}{5}\left(\frac{\rho_f}{\rho_{fb}}\right) \tag{3}$$

Using the balanced reinforcement ratio (ρ_{fb}) in this equation implies that deflection depends on the ultimate tensile stress of the FRP reinforcement.

After cracking, the composite action between the concrete and FRP rebars may not be as perfect as it is usually assumed [7, 12]. In addition, shrinkage and the non-linear behaviour of concrete in the compression zone can affect the stiffness of an RC element [15]. To address this issue, a possible approach is to provide a transition between I_g and a certain fraction of I_{cr} in the calculation of I_e. Such an equation was proposed by Benmokrane et al [12], but was calibrated using a limited number of tests (Equation 4).

$$I_e = \alpha_0 I_{cr} + \left(\frac{I_g}{\beta_0} - \alpha_0 I_{cr}\right)\left[\frac{M_{cr}}{M_a}\right]^3 \tag{4}$$

where α_0 and β_0 are equal to 0.84 and 7, respectively. Naturally, this equation offers more flexibility compared to the current ACI 440.1R-06 [5] equation. The factor α_0 can reflect the reduced composite action between the concrete and FRP rebars. The factor β_0 was introduced in the equation to enable a faster transition from I_g to I_{cr}, since the degradation in stiffness due to the 3rd power component was considered to be too low.

Bischoff [7] and Bischoff and Scanlon [22] analyzed extensively the ACI 318 [6] expression for I_e from a tension-stiffening standpoint. The results of their studies indicate that the ACI 318 [6] proposed method is not suitable for GFRP RC. The following equation was proposed for I_e, which is analogous to the equation that can be deduced by implementing the provisions of CEB-FIP Model Code 90 [3] to determine instantaneous curvatures or deflections. This equation is claimed to be equally applicable for FRP and steel RC beams.

$$I_e = \frac{I_{cr}}{1 - \eta\left(\frac{M_{cr}}{M_a}\right)^2} \le I_g \text{ , and } \eta = 1 - \frac{I_{cr}}{I_g} \tag{5}$$

To predict the deformation of RC beam elements, Eurocode 2 [9] tries to account for the tension stiffening effect based on the CEB-FIP Model Code 90 [3] approach. Based on Eurocode 2 [8], the following equation can be used to calculate the short-term deflection (Δ).

$$\Delta = \beta(\frac{M_{cr}}{M_a})^2 \Delta_g + (1 - \beta(\frac{M_{cr}}{M_a})^2)\Delta_{cr} \quad (6)$$

where Δ_g and Δ_{cr} are the uncracked-state and cracked-state deflections, respectively. The coefficient β is a duration or repetition of load factor (1.0 for short-term loading and 0.5 for sustained or cyclic loading). Equation (5) can be derived directly from equation (6) by using the β value for short-term loading.

3- Experimental programme

The experiments consisted of three series of GFRP and three series of CFRP tests on RC beams and slabs. To ensure repeatability, each series comprised two identical elements (i.e. in total 24 tests). One series of steel RC beams and slabs was also tested for comparison purposes.

3.1. Materials

Aslan 100 CFRP and GFRP rebars were used for the main flexural reinforcement of the beams and slabs. The surface treatment of these rebars is characterized by helically over-wound fibres and sand coating. The tensile properties were obtained by testing a representative number of samples in uni-axial tension, using resin filled steel tubes in the grips, and are shown in Table 1. Most of the bars failed away from the grips, so the results reflect the tensile strength of the composite. It should be noted that the strength of the larger diameter GRFP bars was similar to the strength of the smaller diameter bars, contrary to the manufacturer's supplied data. The steel rebars had a nominal diameter of 12 mm and a mean yield strength of 590 MPa and mean ultimate strength of 675 MPa.

In this study, concrete was produced using 25 mm maximum aggregate size, 0.48 water to cement ratio and 380 kg/m^3 cement content. The fresh concrete slump was about 75 mm, and the average 28-day cube compressive strength and module of elasticity was found to be around 35 MPa and 29500 MPa, respectively.

3.2. Details of beam and slab elements

The beam series were designated as BG#, BC#, BS# and slab series as SG#, SC#, SS#. B and S stand for beam and slab, while G, C and S identify the type of reinforcement used, GFRP, CFRP or steel, respectively. Notation # represents the series number, and the two identical elements within each series are identified by adding a or b to the end of the series name.

The beam elements were 150 mm wide, 250 mm high, 2550 mm long, with the distance between the end-supports being 2300 mm (see Figure 1). The shear span (767 mm) was reinforced with steel stirrups to avoid shear failure, while no shear reinforcement was provided in the constant bending moment zone. GFRP and CFRP rebars with nominal diameter of 6 mm were used as top reinforcement within the shear span to hold the stirrups in place. The clear concrete cover to the main rebars was 25 mm in all cases. Each beam series was designed to be under-reinforced, balanced or over-reinforced, with failure occurring by rupture of bars or crushing of concrete. The geometric and reinforcement details of GFRP and CFRP RC beams are given in Figure 1 and Table 2. The reinforcement ratio of the corresponding beam and slab series is almost identical to enable comparison between the deflection behaviour of beam and slab elements with similar reinforcement ratios.

The slab elements were 500 mm wide, 120 mm high, 2350 mm long, whilst the distance between the end-supports was 2100 mm. The geometric and reinforcement details of the GFRP and CFRP RC slabs are shown in Figure 2 and Table 3. The clear concrete cover to the main rebars was specified at 25 mm. However, the flotation of the FRP mesh reinforcement during casting resulted in slightly different cover values as reported in Table 3. Similar to the beam elements, each slab series had a different reinforcement ratio (under-reinforced, balanced and over-reinforced).

3.3. Instrumentation and Test Procedure

The two elements in each beam and slab series, along with eight control cubes and eight control cylinders were constructed from the same batch of concrete. All the specimens in each series, including the control cubes and cylinders, were cured under similar conditions and tested on the same day. The cubes were used to determine the compressive strength, while the cylinders were used to determine the tensile strength of the concrete according to ASTM C496-96 [23]. Table 4 shows the compressive and tensile strength of concrete for different beam and slab series.

As shown in Figures 1 and 2, the elements were tested under four-point loading. The total load was applied by means of a 600 kN hydraulic actuator and a loading beam was used to subject both beams and slabs to two equal concentrated loads symmetrically placed about mid-span. One rebar of every beam and slab was instrumented with a total of fourteen strain gauges. Four strain gauges were used to evaluate strain development and average bond stresses within the shear span. The other ten strain gauges were concentrated around a crack inducer at mid-span to investigate tension stiffening and bond profiles. Two dial gauges were used to measure settlements at the end supports and five linear variable displacement

transducers (LVDT) were used to measure deflections (Figures 1 and 2). One strain gauge was also used to measure the top surface concrete strain at mid-span. The testing was carried out in displacement control and the load was paused at about 5 kN intervals to mark and measure the cracks and to take notes. Two load cycles were performed for each specimen. In the first cycle, the load was increased to a service load level corresponding to a stress of about 45% of the estimated concrete compressive strength in the top concrete fibre at mid-span. In the second cycle, the load was increased until failure occurred, either by rupture of bars or by crushing of concrete. All data (load, strains and deflections) were collected by a data acquisition system at a sampling frequency of 1Hz.

4- Test results and discussion

Figure 3 shows the experimental load-deflection response at mid-span for all tested beams and slabs. It is clear from this figure that the results of the two replicate elements within each series are very similar. The only exception is in the SC3 series (Figure 3-d), where the clear cover is significantly different for SC3a and SC3b slabs. Therefore, it can be confirmed that in general the materials used, the production of the elements and the test procedure were all well controlled. Due to limitations of space, only some of the results are discussed in this paper in detail. Similar behaviour was observed for all of the tested specimens.

4.1. Modes of failure

The three series of FRP RC beams and slabs were designed to investigate different flexural failure modes including rupture of the rebars (under-reinforced), compressive failure of the concrete (over reinforced) and balanced failure (compressive concrete failure followed immediately by rupture of the rebars). The modes of failure for all tested beam and slab elements are given in Tables 2 and 3. It should be mentioned that under-reinforced FRP RC sections are not usually of interest for design purposes, since the failure is brittle and drastically catastrophic; however, they result in much higher stress levels in the FRP bars which is of interest in terms of deflection behaviour.

4.2. Strain in the concrete and rebars

A cracked-section analysis was performed to estimate the load deflection response of each of the tested specimens. The assumption of plane sections remain plane was implemented in this analysis. A linear elastic behaviour for the FRP reinforcement was considered, while the stress-strain relationship for the concrete in compression was based on the Eurocode 2 model [9]. The concrete was assumed to resist no tension. Typical experimental load-rebar strain relationships for BG2 are shown in Figure 4-a. The

results show that cracked-section analysis predicts reasonably well the maximum rebar strain at the location of the pre-formed crack. Beyond cracking, the rebar strains around the crack inducer follow almost a linear relationship with load up to failure. From the analysis of Figure 4.a it can be seen that cracking at the location of the crack inducer takes place at 13 kN, as captured by gauge No. 10. However, the first natural crack takes place at 18 kN and its development was captured by gauge No. 14. At higher load levels, the natural crack developed wider than the induced crack and hence the rebar undergoes additional strain when moving away from mid-span induced crack.

The load-concrete strain relationships shown in Figure 4-b indicate that the concrete strain at the extreme top fibre (above the location of the crack) considerably exceeds that predicted by cracked-section analysis. This can be attributed to the fact that cracked-section analysis assumes a linear strain distribution in the section that may not be accurate enough for FRP RC beams, as the low modulus of elasticity of FRP rebars leads to wider cracks, and therefore, more localized effects compared to steel RC beams.

4.3. Curvature

FRP rebars have high tensile strength and their stress-strain behaviour is linear up to failure. Using the experimental top-fibre concrete strain (ε_c), an average of the rebar strains around the crack inducer (ε_{fave}), and the effective reinforcement depth (d), the curvature (ϕ) at every load level was evaluated from the test results according to the general approach of CEB, as follows.

$$\varphi = \frac{\varepsilon_c + \varepsilon_{fave}}{d} \tag{7}$$

The experimentally derived load-curvature relationships, in general, compare well to those derived by cracked-section analysis (Figure 5-a). In this study, the experimentally derived moment-curvature relationships were used to calculate the mid-span deflections that are associated with the flexure behaviour as shown in Figure 5-b. It can be seen that for SG2 (balanced reinforced slab) the measured deflections are larger than the predicted flexural deflections, and they start to deviate shortly after shear cracking (14.8 kN). The difference between the measured and flexural deflections can be investigated further by examining the strain profiles along the rebar at different load levels. The small difference in the cracking loads observed in Figures 5-a and 5-b is attributable to the fact that deflections are affected by localised effects to a lesser extent than section curvatures. Figure 6 shows the experimental profile of strains along a rebar in slab element SG2. Any noticeable increase in the rebar strain is caused by the

development of a nearby crack (i.e. mid-span induced crack and adjacent cracks). The strain profiles along the rebar in the shear span indicate that the rebar undergoes additional strains, in excess of the strains due to flexure, since the strains at the centre span are lower than in the region near the loading points. This behaviour is not observed in steel RC since the considerably higher steel stiffness controls crack widths and restricts the spread of additional deformations. In other words, due to the low modulus of elasticity of the FRP rebars (especially GFRP rebars), the contribution of shear and bond-slip induced deformations could be of major significance for FRP RC elements. For example, this additional deflection for beam BG2 was estimated to be 20% of the measured deflection at failure [16].

4.4. Deflection

Calculated load-mid-span flexural deflections of beams BG1a (low reinforcement ratio) and BG3a (high reinforcement ratio) are compared to the measured deflections in Figure 7. Figure 8 shows the calculated flexural deflections and experimental measured deflections of their corresponding slab elements SG1a (low reinforcement ratio) and SG3a (high reinforcement ratio).

As shown in Figures 7-a and 8-a, the effect of the additional component of the mid-span deflection is not prominent for series BG1 and SG1 (low reinforcement ratio elements) because premature failure occurred by rupture of the rebars, when the load level was relatively low. For BG3 and SG3 (Figures 7-b and 8-b) the high amount of reinforcement could provide better control over the additional deformations (shear or bond-slip induced deformations) at the lower load levels. As a result, the additional deflections were observed at the higher load level. It is therefore suspected that the additional deformations are more important in beams and slabs with a moderate reinforcement ratio (see Figure 5-b). Based on the above discussion, for GFRP RC elements with moderate to high reinforcement ratios, it would be important to evaluate the additional deformations [16].

5. Prediction of deflection

Figures 9 to 12 compare experimental mid-span deflections for all tested beams and slabs to the deflections predicted using different simple prediction equations. It should be noted, the results of this study showed that, in general, the accuracy of the predicted deflection is highly dependent on the accuracy of the calculated cracking moment. Accurate estimation of concrete cover is also important for thin RC slabs where a small variation in the concrete cover would result in a considerable variation in the cracked moment of inertia. To better evaluate the accuracy of different analytical methods, the ratio of the

analytical to the experimental mid-span deflection was calculated for all FRP RC elements at both service and ultimate limit states (Table 5). In the present study, the service load is that corresponding to a stress level in the top concrete fibre of about 40% of the concrete compressive strength.

5.1. Service limit state

The results show that ACI 440.1R-06 [5] approach, in general, overestimates deflections (up to 18%) for FRP RC elements with low reinforcement ratio (beams: BG1 and BC1; slabs: SG1 and SC1) at service limit state. However, for FRP RC beams and slabs with moderate to high reinforced ratio this method always underestimates the service level deflections (on average by 11% and 34% for FRP reinforced beams and slabs, respectively).

As mentioned before, the effective moment of inertia (I_e) proposed by Bischoff [7] and Eurocode 2 [9] are both based on the tension stiffening provisions of CEB-FIP Model Code 1990 [3]; and therefore, lead to identical deflection predictions. Figures 9 to 12 show that the deflections predicted according to Eurocode2 [9] and Bischoff [7] approach in general compare well with the measured deflections at low load levels. However, the predicted deflections for the FRP RC elements were on average 17% less than the measured deflections.

Benmokrane et al [12] equation is found to considerably overestimate (up to 42%) the deflection of FRP RC beams and slabs at service load level (see Table 5). The reason could be attributed to the use of β_0 factor in this equation that leads to a high degradation in stiffness at service load level as shown in Figures 9 to 12.

5.2. Ultimate limit state

The results of this study indicate that both ACI 440.1R-06 [5] and Eurocode 2 [9] (and Bischoff [7]) equations underestimate the measured deflections of FRP RC elements by up to 25% at high levels of load. Table 5 indicates that predicted mid-span deflections are on average 12% and 20% less than the measured deflections of low and moderate to high reinforced ratio FRP RC elements, respectively. As discussed in previous sections, the difference between the calculated and measured deflections in moderate to high reinforced ratio FRP RC elements may be mainly attributed to the additional deformations induced by shear and bond-slip. It is shown in Figures 9 to 12 that, except for two GFRP RC slabs (SG1and SG3), Benmokrane et al [12] proposed method was fairly accurate in predicting the ultimate mid-span deflection of FRP RC elements. Table 5 shows that this method underestimates the ultimate deflection of Slab SG1 by 37% and overestimates the ultimate deflection of Slab SG3 by 23%.

The results of this study indicate that additional deformations other than those induced by pure flexure could be significant particularly in FRP RC beams and slabs with moderate to high reinforced ratio. However, it seems that most of the existing simplified methods to predict deflections of FRP RC elements do not adequately take into account these additional deformations. This usually leads to un-conservative predictions especially at higher load levels. It should be mentioned that additional deformations may not always be significant at the serviceability load. Nevertheless, it is still important to predict deformation of FRP RC elements over the entire loading range with good accuracy. This requires developing more fundamental methods to evaluate shear and bond-slip induced deflections [24, 25]. Further analytical investigations will be published by the authors in a separate, forthcoming paper.

6- Conclusions

This study experimentally investigated the deflection behaviour of 24 GFRP and CFRP RC beams and slabs covering a wide range of reinforcement ratios. Based on the results, the following conclusions can be drawn:

- For FRP RC beams and slabs, the plain section remains plain assumption across the entire section may not be valid for high levels of loading.
- Existing approaches to estimate deflections of RC elements by considering solely their flexural behaviour tend to underestimate overall deformations. The contribution to overall deflections of other possible stiffness-reducing mechanisms (e.g. shear cracking, shrinkage and loss of bond) can be significant, particularly in FRP RC elements having moderate to high reinforcement ratios and should be further investigated. The accuracy of the predicted deflection for FRP RC elements (particularly in thin slabs) is highly dependent on the accuracy of the calculated cracking moment and concrete cover.
- The ACI 440.1R-06 [5] equation leads to overestimated service level deflections at low reinforced ratios, and underestimated deflections at moderate to high reinforced ratio FRP RC beams and slabs. This method underestimates the measured ultimate deflections especially for moderate to high reinforced ratio FRP RC elements.
- The faster transition to a fully cracked response assumed in the model proposed by Benmokrane et al [12] can overestimate service deflections, especially for moderate to high reinforcement ratios.

- The performance of the approach recommended in Eurocode 2 [9] and the analogous model proposed by Bishoff [7] offer more consistent predictions throughout the range of reinforcement ratios explored in this experimental programme. These methods, however, tend to underestimate deflections at service load (on average by 17%) and to a larger extent at ultimate limit states, especially for moderate to high reinforced ratio (up to 25%).

References

[1] Gdoutos A, Pilakoutas K, Rodopoulos C (Eds), Failure Analysis of Industrial Composite Materials, McGraw-Hill Professional Engineering, New York, 2000. p.51-108.

[2] Pilakoutas K, Neocleous K, Guadagnini M. Design philosophy issues of fiber reinforced polymer reinforced concrete structures. Journal of Composites for Construction 2002; 6(3): 154-161.

[3] CEB. CEB-FIP Model Code 1990. Comite Euro-International du Beton, Thomas Telford Ltd, 1993.

[4] *fib* Bulletin No. 40, FRP Reinforcement in RC Structures, International Federation for Structural Concrete, Lausanne, Switzerland, 2007.

[5] ACI Committee 440. Guide for the Design and Construction of Concrete Reinforced with FRP Bars (ACI 440.1R-06). American Concrete Institute, Farmington Hills, 2006.

[6] ACI Committee 318. Building Code Requirements for Structural Concrete (ACI 318-08) and Commentary (ACI 318R-08). American Concrete Institute, Farmington Hills, Mich, 2008.

[7] Bischoff PH. Deflection Calculation of FRP Reinforced Concrete Beams Based on Modifications to the Existing Branson Equation. Journal of Composites for Construction 2007; 11(1): 4-14.

[8] ISIS Canada. Reinforcing Concrete Structures with Fibre Reinforced Polymers-Design Manual No. 3. ISIS Canada Corporation, University of Manitoba, Winnipeg, Manitoba, Canada, 2001.

[9] CEN. Eurocode 2: Design of concrete structures - Part 1-1: General rules and rules for buildings (EN 1992-1-1:2004). European Committee for Standardisation, 2004.

[10] CAN/CSA-S806. Design and Construction of Building Components with Fibre-Reinforced Polymers. Canadian Standards Association, Mississauga, Ontario, Canada, 2002.

[11] Achillides Z, Pilakoutas K.. Bond behaviour of fiber reinforced polymer bars under direct pullout conditions, Journal of Composites for Construction 2004; 8 (2): 173-181.

[12] Benmokrane B, Chaallal O, Masmoudi R. 1996, Flexural Response of Concrete Beams Reinforced with FRP Reinforcing Bars, ACI Structural Journal 1996; 93(1): 46-55.

[13] Wei Z. Crack and Deformation Behaviour of FRP Reinforced Concrete Structures. PhD thesis, the

University of Sheffield, Sheffield, UK, 1999.

[14] Al-Sunna R., Pilakoutas K, Waldron P, Al-Hadeed T. Deflection of FRP reinforced concrete beams, In: 4th Middle East Symp. on Structural Composites for Infrastructure Applications (MESC-4), Alexandria, Egypt, 2005.

[15] Bischoff PH, Johnson RD. Effect of shrinkage on short-term deflections of reinforced concrete beams and slabs. ACI Structural Journal 2008, 105 (4): 516 – 518.

[16] Al-Sunna R. Deflection Behaviour of FRP Reinforced Concrete Flexural Members, PhD thesis, the University of Sheffield, Sheffield, UK, 2006.

[17] Mota C, Alminar S, Svecova D, Critical Review of Deflection Formulas for FRP-RC Members. Journal of Composites for Construction, ASCE 2006; 10 (3): 183-194.

[18] Rafi MM, Nadjai A, Evaluation of ACI 440 deflection model for fiber-reinforced polymer reinforced concrete beams and suggested modification, ACI Structural Journal 2009; 106 (6): 762-771.

[19] Masmoudi, R., Theriault, M., and Benmokrane, B. Flexural behavior of concrete beams reinforced with deformed fiber reinforced plastic reinforcing rods, ACI Structural Journal 1998; 95(6): 665 – 675.

[20] Yost, J. R., Gross, S. P., and Dinehart, D. W. Effective moment of inertia for glass fiber-reinforced polymer-reinforced concrete beams. ACI Structural Journal 2003; 100(6): 732 – 739.

[21] ACI Committee 440. Guide for the Design and Construction of Concrete Reinforced with FRP Bars, (ACI 440.1R-03). American Concrete Institute, Farmington Hills, 2003.

[22] Bischoff PH, Scanlon A. Effective moment of inertia for calculating deflections of concrete members containing steel reinforcement and fiber-reinforced polymer reinforcement. ACI Structural Journal 2007; 104(1): 68-76.

[23] ASTM C496-96 Standard Test Method for Splitting Tensile Strength of Cylindrical Concrete Specimens, ASTM Committee, Philadelphia, 1996.

[24] Guadagnini M, Pilakoutas K, Waldron P. Shear resistance of FRP RC beams: Experimental study. Journal of Composites for Construction 2006; 10 (6): 464-473.

[25] Imjai, T., Guadagnini, M. and Pilakoutas K. Estimation of Shear Crack Induced Deformations of FRP RC Beams, 9th International Symposium on Fiber Reinforced Polymer Reinforcement for Concrete Structures, Sydney, Australia, 2009.

Table 1. Tensile properties of GFRP and CFRP rebars.

Rebar Type	Nominal diameter (mm)	Manufacturer modulus of elasticity (MPa)	Test modulus of elasticity (MPa)	Manufacturer guaranteed tensile strength (MPa)	Test tensile strength, (MPa)	
					Average	Standard Deviation
GFRP	6.35	40800	38900	830	600	70
	9.53	40800	42800	760	665	35
	12.7	40800	41600	690	620	40
	19.05	40800	42000	620	670	10
CFRP	6.35	120000	133000	1450	1450	40
	9.53	123000	132000	1380	1320	170
	12.7	112000	119000	1230	1475	60

Table 2. Reinforcement details of the test beams

Series Designation		Beam Designation	Rebar Details	Reinforcement Ratio	Type of Failure
GFRP Beams	BG1	BG1a	2Φ9.53	0.0043	Rupture of rebars
		BG1b			
	BG2	BG2a	2Φ12.7	0.0077	Almost balanced
		BG2b			
	BG3	BG3a	4Φ19.05 (1)	0.0391	Concrete crushing
		BG3b			
CFRP Beams	BC1	BC1a	3Φ6.35	0.0029	Rupture of rebars
		BC1b			
	BC2	BC2a	3Φ9.53	0.0065	Almost balanced
		BC2b			
	BC3	BC3a	3Φ12.7	0.0116	Concrete crushing
		BC3b			
Steel Beams	BS	BSa	2Φ12	0.0069	Yielding of reinforcement
		BSb			

(1) Two layers, with 25 mm clear spacing between them.

Table 3. Reinforcement details of the test slabs

Series Designation		Slab Designation	Cover (mm)	Main Rebar	Transverse Rebar	Reinforcement Ratio	Type of Failure
GFRP Slabs	SG1	SG1a	27.5	5Φ6.35	7Φ9.53 /m	0.0035	Rupture of rebars
		SG1b	27.5				
	SG2	SG2a	31	5Φ9.53	7Φ9.53 /m	0.0079	Almost balanced
		SG2b	31				
	SG3	SG3a	40	5Φ19.05	7Φ9.53 /m	0.0333	Concrete crushing
		SG3b	40				
CFRP Slabs	SC1	SC1a	31	4Φ6.35	6Φ6.35 /m	0.0028	Rupture of rebars
		SC1b	33				
	SC2	SC2a	38	4Φ9.53	6Φ6.35 /m	0.0063	Almost balanced
		SC2b	35				
	SC3	SC3a	42.5	4Φ12.7	6Φ6.35 /m	0.0114	Concrete crushing
		SC3b	36				
Steel Slabs	SS	SSa	25	4Φ10	5Φ8 /m	0.0070	Yielding of reinforcement
		SSb	25				

Table 4. Mechanical properties of the concrete

Series Designation		Cube Compressive Strength (MPa)		Split Cylindrical Tensile Strength (MPa)	
		Average	Standard Deviation	Average	Standard Deviation
GFRP Beams	BG1	47.7	3.56	4.1	0.29
	BG2	47.7	3.56	3.8	0.15
	BG3	46.5	0.92	3.6	0.08
CFRP Beams	BC1	55.4	2.86	3.9	0.20
	BC2	52.6	2.38	3.6	0.05
	BC3	51.8	2.59	3.6	0.19
Steel Beams	BS	52.0	1.40	4.1	0.28
GFRP Slabs	SG1	51.0	1.44	3.9	0.23
	SG2	46.2	1.55	3.4	0.24
	SG3	45.9	2.02	3.8	0.17
CFRP Slabs	SC1	50.1	2.50	3.9	0.21
	SC2	51.0	2.41	3.4	0.11
	SC3	49.8	3.95	3.8	0.24
Steel Slabs	SS	50.6	2.56	3.6	0.24

Table 5. Analytical to experimental mid-span deflection for FRP reinforced elements

Series Designation		Load State	Ratio of analytical to experimental mid-span deflection					
			ACI 440.1R- 06		Eurocode 2, Bischoff		Benmokrane	
CFRP Beams	BC1	Service	1.13		0.75		1.21	
		Ultimate	0.95		0.90		1.13	
	BC2	Service	0.90		0.78		1.15	
		Ultimate	0.80		0.78		0.95	
	BC3	Service	0.88		0.87		1.25	
		Ultimate	0.76		0.75		0.90	
GFRP Beams	BG1	Service	1.14		0.76		1.15	
		Ultimate	0.84		0.81		0.97	
	BG2	Service	0.89		0.81		1.28	
		Ultimate	0.77		0.75		1.01	
	BG3	Service	0.87		0.86		1.34	
		Ultimate	0.79		0.79		0.95	
CFRP Slabs	SC1	Service	1.08		0.73		1.13	
		Ultimate	0.92		0.88		1.08	
	SC2	Service	0.61		0.72		1.05	
		Ultimate	0.83		0.82		1.01	
	SC3	Service	0.71		0.81		1.13	
		Ultimate	0.82		0.85		1.11	
GFRP Slabs	SG1	Service	1.18		0.95		1.10	
		Ultimate	0.79		0.93		0.63	
	SG2	Service	0.66		0.92		1.24	
		Ultimate	0.79		0.84		1.06	
	SG3	Service	0.65		0.97		1.42	
		Ultimate	0.84		0.86		1.23	
Average			0.89	0.83	0.83	0.83	1.20	1.00
Standard Deviation			0.20	0.06	0.09	0.06	0.11	0.15

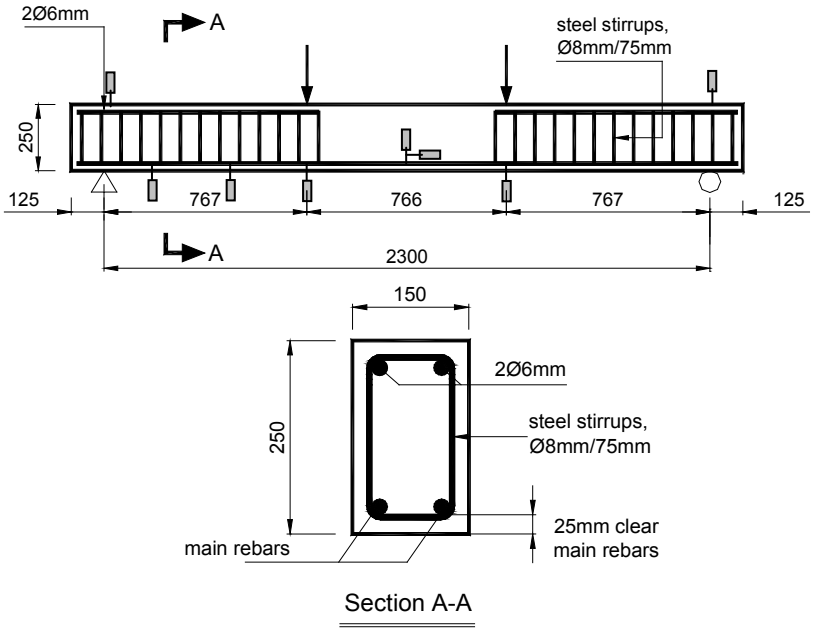

Figure 1. Geometric and reinforcement details of the test beams

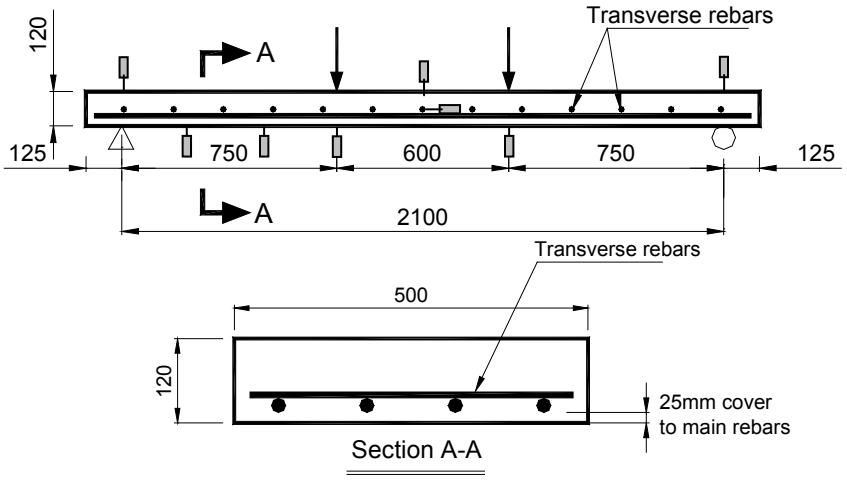

Figure 2. Geometric and reinforcement details of the test slabs

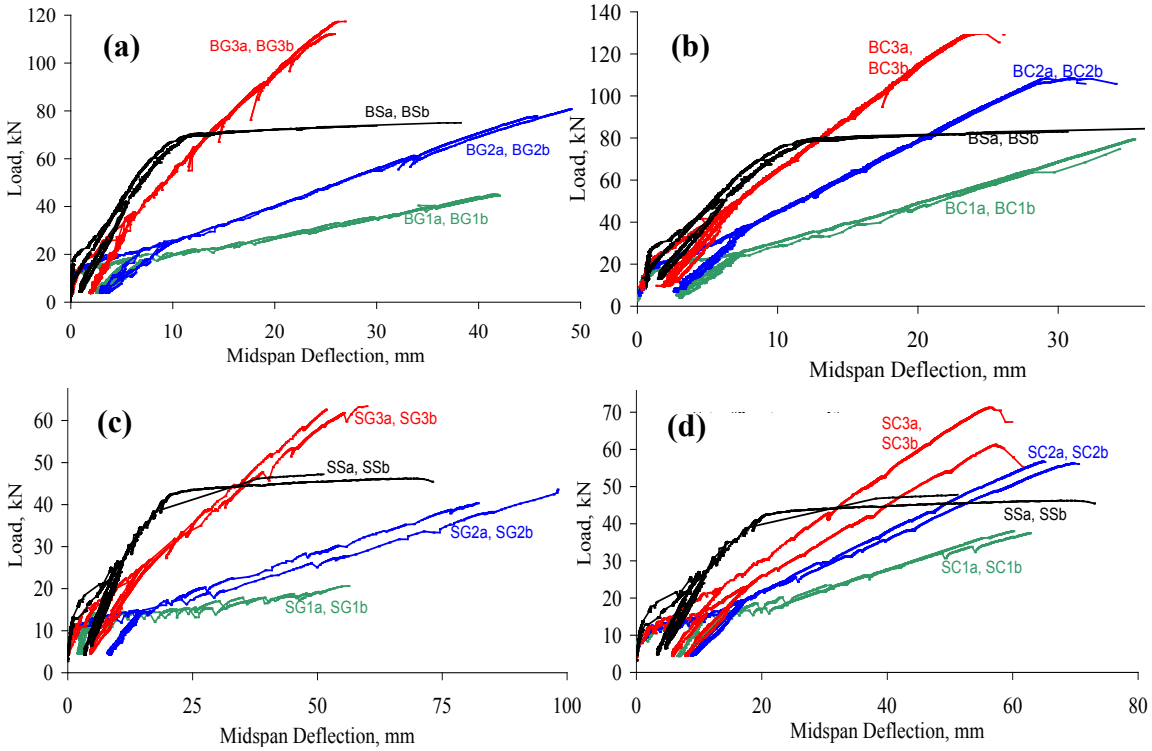

Figure 3. Experimental load vs. mid-span deflection; series (a): BG, (b): BC, (c): SG, (d): SC

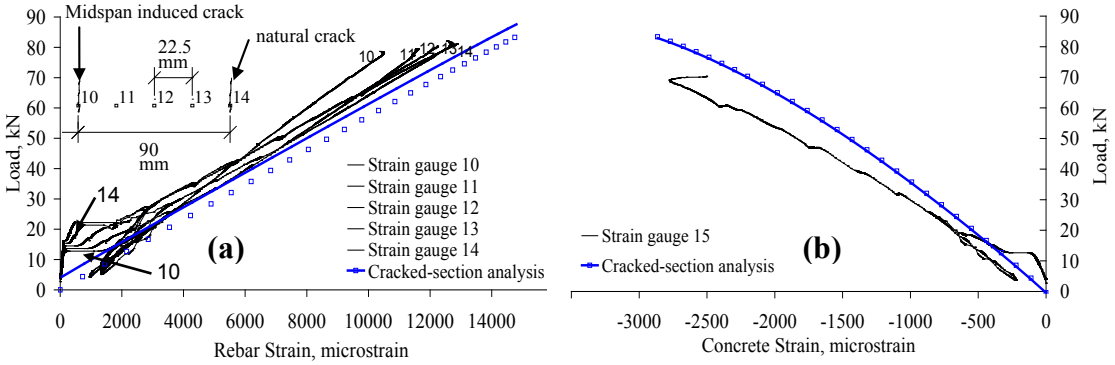

Figure 4. Typical experimental load vs. strain relationships for beam BG2; (a): Rebar strain; (b): Concrete strain

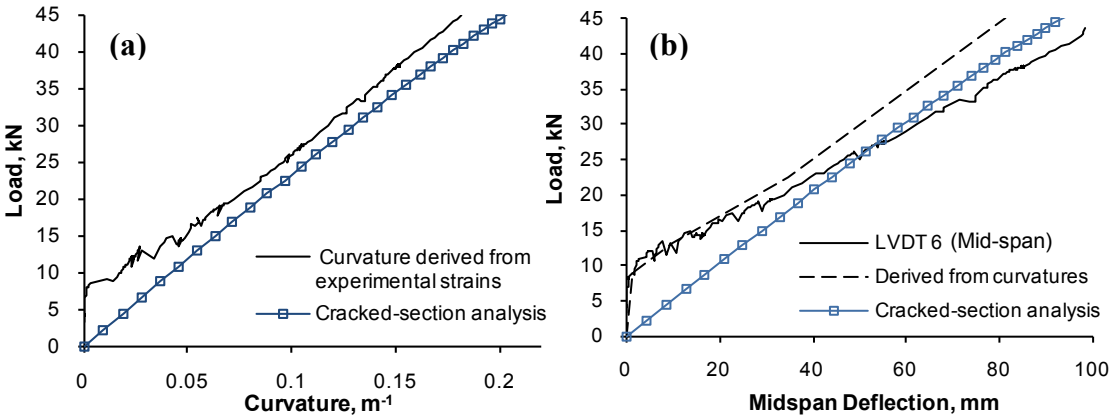

Figure 5. Typical experimental load vs. (a): curvature, and (b): mid-span deflection, slab SG2a

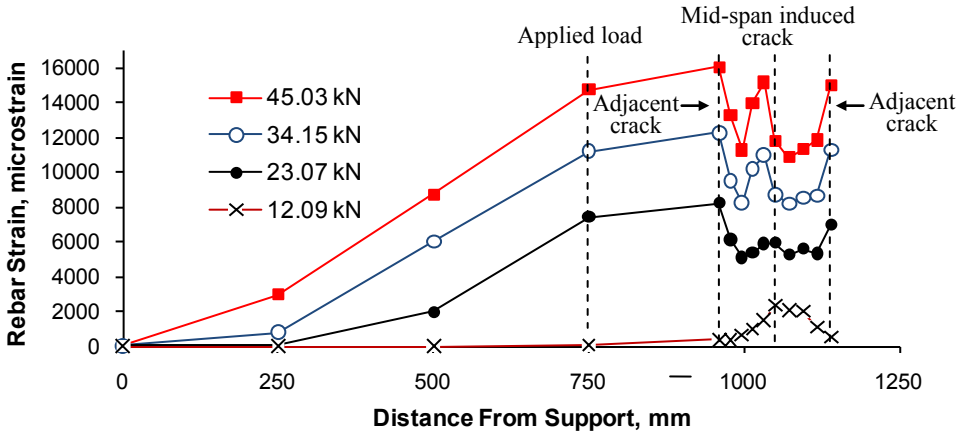

Figure 6. Typical experimental profile of strains along a rebar, SG2

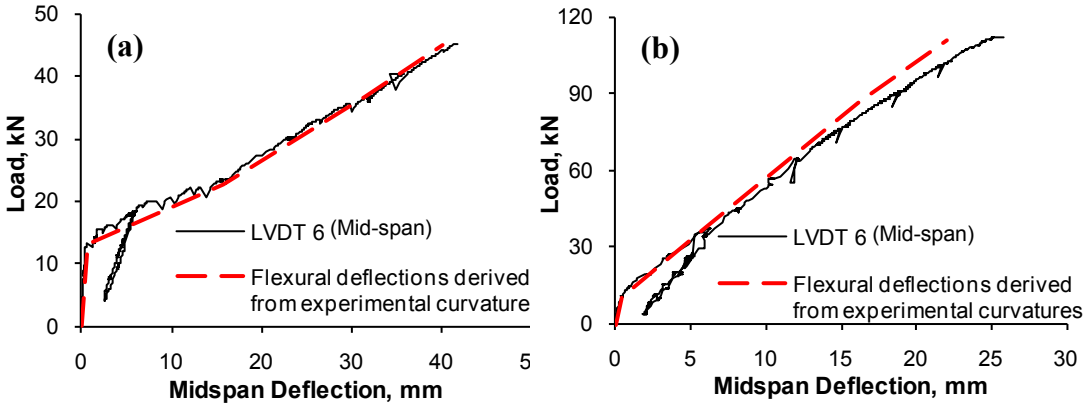

Figure 7. Experimental load vs. mid-span deflection for (a): BG1, and (b): BG3

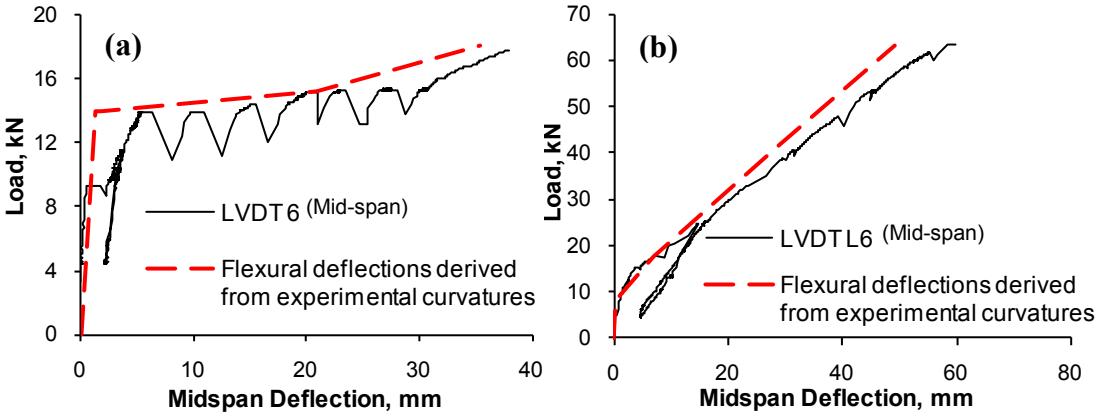

Figure 8. Experimental load vs. mid-span deflection for (a): SG1, and (b): SG3

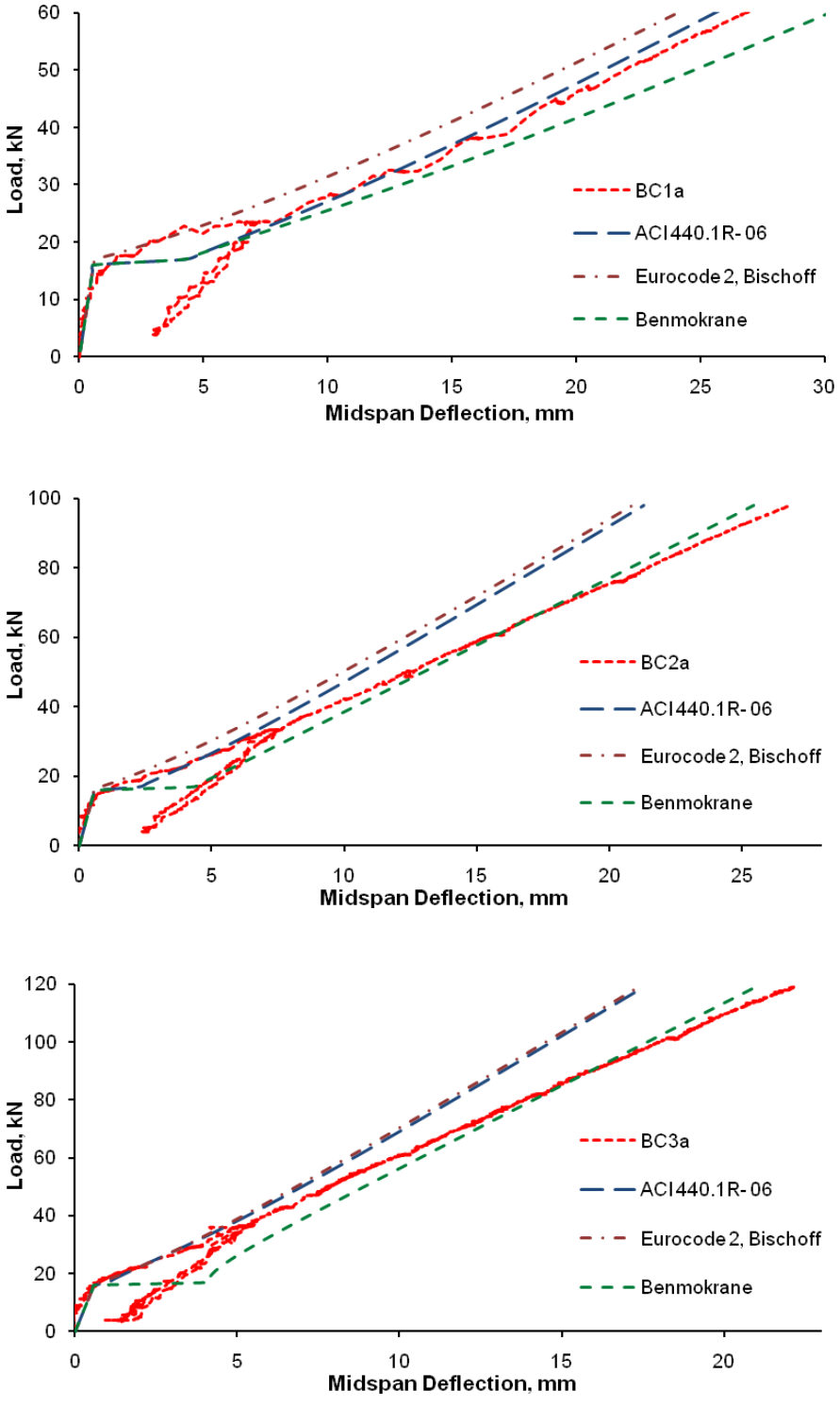

Figure 9. Experimental and predicted deflections – CFRP beams

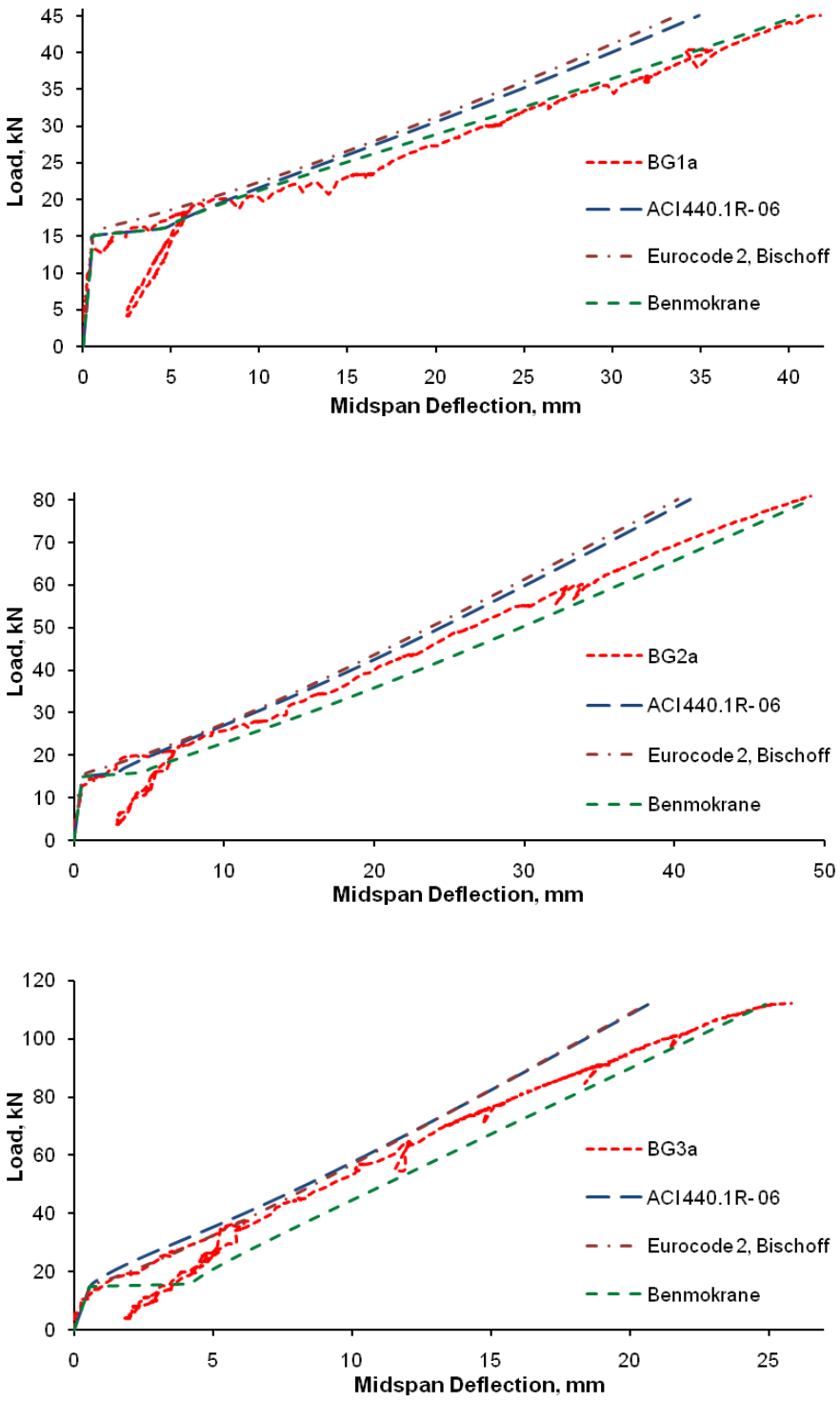

Figure 10. Experimental and predicted deflections – GFRP beams

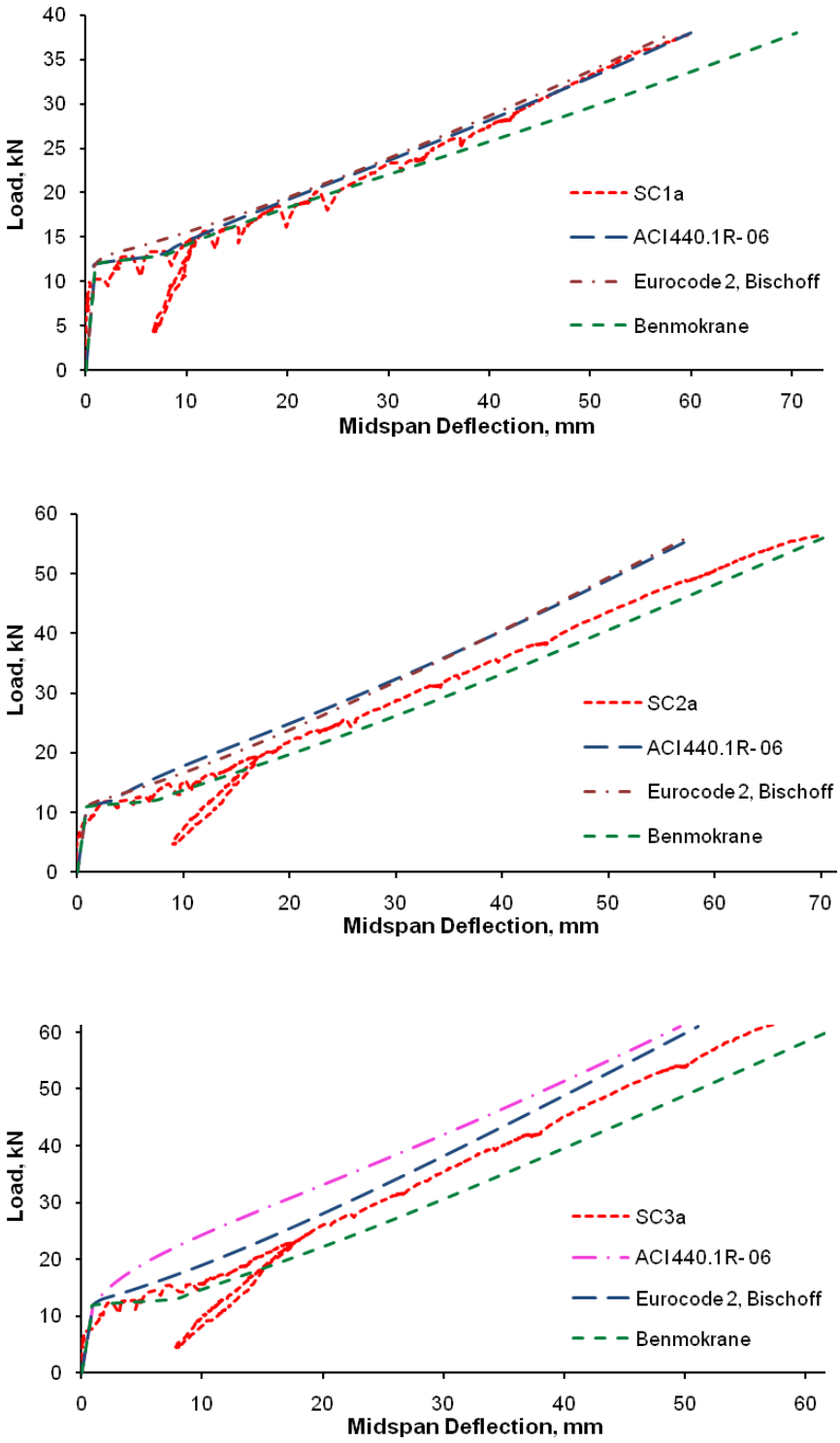

Figure 11. Experimental and predicted deflections – CFRP slabs

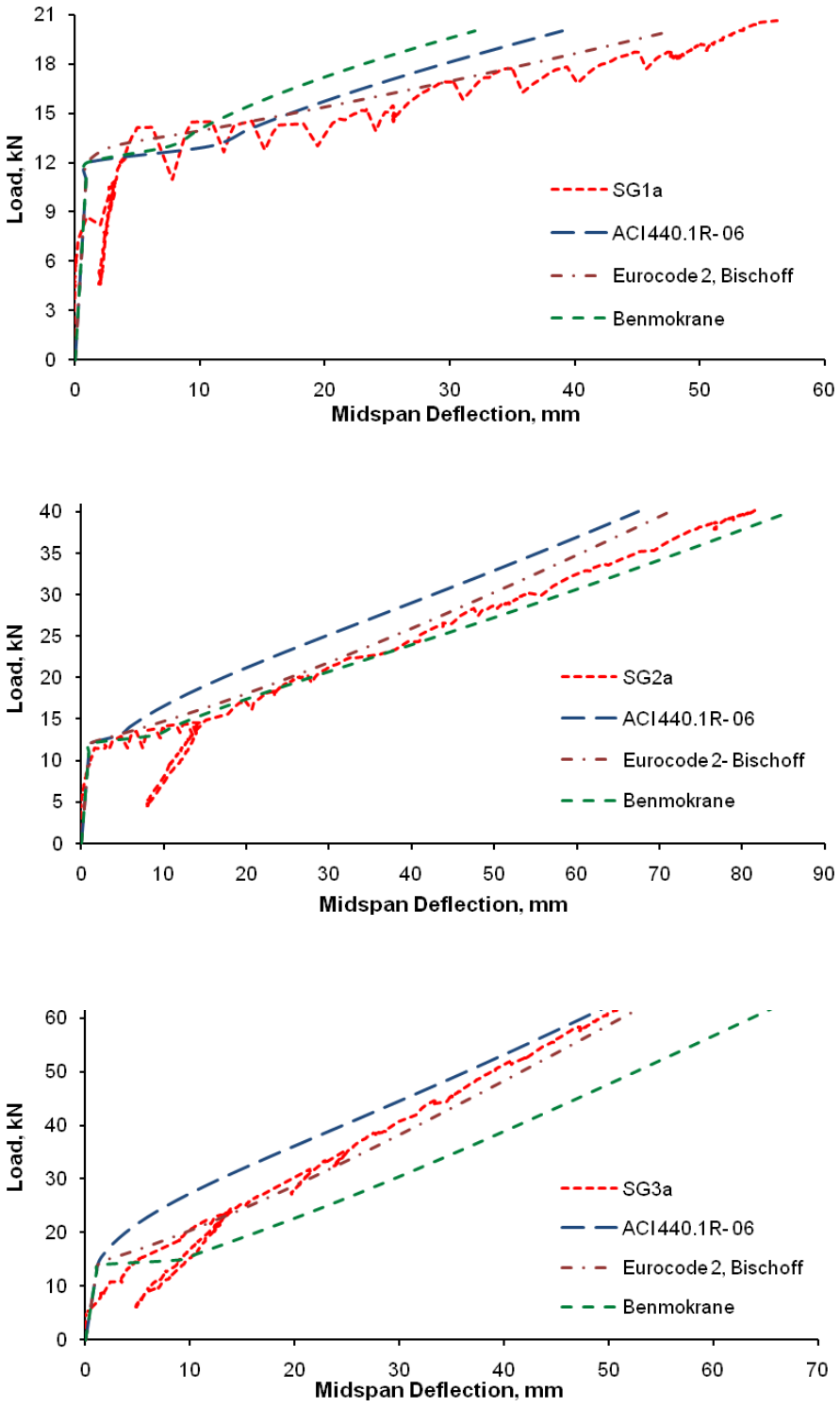

Figure 12. Experimental and predicted deflections – GFRP slabs